Thermal conductivity of cubic and hexagonal mesoporous silica thin films

Thomas Coquil,[1] Erik K. Richman,[2] Neal J. Hutchinson,[1] Sarah H. Tolbert,[2,a)] and Laurent Pilon[1,b)]
[1]*Mechanical and Aerospace Engineering Department, Henry Samueli School of Engineering and Applied Sciences, University of California, Los Angeles, 420 Westwood Plaza, Los Angeles, California 90095, USA*
[2]*Department of Chemistry and Biochemistry, University of California, Los Angeles, 607 Charles E. Young Drive East, P.O. Box 951569, Los Angeles, California 90095-1569, USA*

(Received 26 March 2009; accepted 24 May 2009; published online 10 August 2009)

This paper reports the cross-plane thermal conductivity of highly ordered cubic and hexagonal templated mesoporous amorphous silica thin films synthesized by evaporation-induced self-assembly process. Cubic and hexagonal films featured spherical and cylindrical pores and average porosities of 25% and 45%, respectively. The pore diameters ranged from 3 to 18 nm and film thickness from 80 to 540 nm, while the average wall thickness varied from 3 to 12 nm. The thermal conductivity was measured at room temperature using the 3ω method. The experimental setup and the associated analysis were validated by comparing the thermal conductivity measurements with the data reported in literature for the silicon substrate and for high quality thermal oxide thin films with thicknesses ranging from 100 to 500 nm. The cross-plane thermal conductivity of the synthesized mesoporous silica thin films does not show strong dependence on pore size, wall thickness, or film thickness. This is due to the fact that heat is mainly carried by very localized nonpropagating vibrational modes. The average thermal conductivity for the cubic mesoporous silica films was 0.30 ± 0.02 W/m K, while it was 0.20 ± 0.01 W/m K for the hexagonal films. This corresponds to reductions of 79% and 86% from bulk fused silica at room temperature. © *2009 American Institute of Physics*. [DOI: 10.1063/1.3182826]

I. INTRODUCTION

Mesoporous silica is one of the potential ultra-low-k dielectric interlayer materials that fulfills the requirements of the International Technology Roadmap for Semiconductors 2006 update.[1] The objective is to synthesize dielectric materials with dielectric constant less than 2.0 to further enhance the signal propagating speed by reducing the R_eC time delay constant.[2] The resistance R_e has already been reduced by replacing aluminum-alloy wires by copper interconnects.[3] On the other hand, the capacitance C between adjacent metal wires can be reduced by introducing nanopores in a dielectric matrix made of silicon dioxide or polymers.[4–6] Over the past 40 years, Moore's law has successfully predicted that the density of transistors on a computer chip would double every 18–24 months.[7] With rapid increases in device density, the heat flux is constantly increasing while the operating temperature must remain below 85 °C.[8] Thus, thermal management of a central processing unit becomes a major technological challenge. However, by introducing nanoscale pores into the dielectric material, not only the effective dielectric constant but also the thermal conductivity substantially decreases. In this case, the ultra-low-k dielectric material acts as a thermal insulator and may constitute a barrier to efficient heat removal.

Mesoporous silica thin films can also be used for thermal insulation in infrared detectors[9] or various micro-electro-mechanical systems (MEMS). Thus, knowledge of the thermal conductivity of mesoporous dielectric thin films is essential for the design and thermal management of the overall device.

In this manuscript, thermal characterization of cubic and hexagonal mesoporous amorphous silica thin films with various pore sizes and shapes, porosities, morphologies, and thicknesses is presented. First, synthesis and characterization of the mesoporous silica thin films are described in detail. Then, the experimental setup and the associated analysis for measuring the cross-plane thermal conductivity of the synthesized films are presented. Finally, the cross-plane thermal conductivity of all samples is reported and discussed.

II. CURRENT STATE OF KNOWLEDGE

Nanoporous materials can be classified into three groups according to their pore diameter.[10] Microporous material consists of pores with diameters less than 2 nm. The pores of mesoporous materials are 2–50 nm in diameter while they are larger than 50 nm in macroporous materials. This study focuses on mesoporous thin films and only related literature is reviewed.

Mesoporous silica (SiO_2) thin films are of particular interest because of the simplicity of their synthetic process which allows one to easily vary the pore shape and size, the porosity, and the pore spatial arrangement.[11] Two of the most common methods for producing mesoporous thin films are

a)Tel.: +1 (310)-206-4767. FAX: +1 (310)-206-4038. Electronic mail: tolbert@chem.ucla.edu.
b)Tel.: +1 (310)-206-5598. FAX: +1 (310)-206-2302. Electronic mail: pilon@seas.ucla.edu.

(i) aerogel and xerogel processes[12–14] and (ii) surfactant-templating processes based on solution phase self-assembly of surfactant (or block copolymer) micelles with SiO_2 precursor.[15–20] In these approaches, nanosize pores are incorporated in a SiO_2 matrix. The dielectric constant of the nanoporous materials can then be tailored by controlling the porosity.[21]

Beside the low dielectric constant, the nanoporous material to be implemented in integrated circuit (IC) processes must have an adequate mechanical strength to endure the metallization and planarization processes.[21,22] Both aerogel and xerogel have very low dielectric constants ranging from 1.1 to 1.5 at porosity between 85% and 99%.[23] However, they are not suitable for IC integration because (i) they are very fragile[23] and (ii) their synthesis methods are not compatible with existing IC processes.[22] During the past decade, closed-cell polymeric nanofoams with better mechanical stability have been identified as a potential solution.[5,6,23] However, polymeric nanofoams tend to have a lower thermal conductivity compared to porous SiO_2 with the same dielectric constant. Indeed, the thermal conductivity of dense polymer is as low as that of typical porous SiO_2.[24] On the other hand, Baskaran *et al.*[4] reported that surfactant templated mesoporous silica thin films have an elastic modulus satisfying the IC process requirements.

In addition to the mechanical strength and process compatibility, the pore diameter of the porous dielectric material should be smaller than the device feature size[23] predicted to be reduced to 13 nm by 2013.[1] Also, nanoporous materials with monodisperse pore size are preferred in order to tune the effective properties of the material and obtain films with uniform properties. Typical pore diameter of aerogel and xerogel ranges from 10 to 20 nm with broad pore size distribution.[25,26] By contrast, the pore size distribution of the templated mesoporous silica is very narrow with an average diameter that can be less than 5 nm.[4] Furthermore, the effective dielectric constant of templated mesoporous silica thin films can be further optimized by controlling both pore diameter and spatial arrangement.[22]

The thermal conductivity of bulk silica aerogels, xerogels, and Vycor glasses, featuring a wide range of porosity and pore size distribution has been investigated extensively. Scheuerpflug *et al.*[27] measured the thermal conductivity and heat capacity between 1.4 and 300 K of several base catalyzed aerogels with densities from 71 to 262 kg/m^3. Einarsrud *et al.*[12] reported the thermal conductivity at 45 °C of bulk silica aerogels and xerogels obtained by measuring the surface temperature of a heated sample using an infrared camera. The porosity and average pore diameter of the aerogels were 90% and 50 nm, respectively. The porosity and pore diameter of the xerogels ranged from 70% to 81% and from 7 to 20 nm, respectively.[12] Moreover, Jain *et al.*[13] found that the synthesis method for SiO_2 xerogels could affect the thermal conductivity of the film with thickness ranging from 500 nm to 2.5 μm while the porosity varied from 25% to 80% and pore diameter from 1 to 25 nm.[13] Hu *et al.*[14] measured the thermal conductivity at room temperature of 600 nm thick silica xerogels as a function of porosity ranging from 48% to 77% while Delan *et al.*[24] reported the thermal conductivity of SiO_2 aerogel thin films with 55% porosity and film thicknesses equal to 551 and 583 nm. Moreover, Tsui *et al.*[2] reported the in-plane and cross-plane thermal conductivities of spin coated porous silica thin films. The films investigated varied in terms of thickness from 314 to 671 nm and porosity from 21% to 64% and showed a decreasing thermal conductivity with increasing porosity. In addition, Cahill *et al.*[28,29] reported the thermal conductivity of Vycor glass as a function of temperature between 30 and 500 K. The sample porosity and pore diameter were estimated to be 30% and 10 nm, respectively. Watson and Pohl[30] also presented a literature review and measurements of the thermal conductivity of high porosity Vycor glass from 0 to 300 K.

Open pores Dow-Corning extra low k (XLK) dielectric films, synthesized from hydrogen silsesquioxane with average pore diameter around 3 nm and a porosity estimated at 59% were studied by Jin and Wetzel[31] and Costescu *et al.*[32] The thermal conductivity of XLK between 89 and 400 K was found to be about height times smaller than that of dense SiO_2 (Ref. 32) and equal to 0.22 W/m K at room temperature.[31] Delan *et al.*[24] also measured the thermal conductivity of templated mesoporous SiO_2 films at room temperature with thicknesses equal to 385 and 392 nm and film porosity of 52%. Finally, Choi *et al.*[9] recently measured the thermal conductivity of a single 150 nm thick porous templated mesoporous SiO_2 film with 30% porosity.

Nanoporous thin films with matrices other than SiO_2 have also been synthesized and thermally characterized. The thermal conductivity of sintered porous silicon freestanding films, 3–27 μm in thickness with porosity between 27% and 66%, was reported by Wolf and Brendel.[33] They observed an effective thermal conductivity independent of thickness but decreasing as porosity increases. The latter study can be compared to that of Gomes *et al.*,[34] where thermal conductivity of mesoporous silicon thin films with porosities ranging from 30% to 80% and thicknesses from 0.1 to 8 μm was measured by scanning thermal microscopy. Finally, nanoporous bismuth thin films of porosity and thickness ranging between 11% and 50% and 18 and 200 nm, respectively, were studied by Song *et al.*[35] Pore diameter varied between 5 and 10 nm and observations showed that the effective cross-plane thermal conductivity appeared to be less sensitive to porosity than thickness. The reported experimental data for aerogel,[24] xerogel,[13,14] Vycor glass,[36] templated mesoporous silica,[2,24] and nanoporous bismuth[35] were all obtained using the 3ω method.[36]

In brief, aerogels and xerogels thin films display a wider range of porosities and often significantly lower thermal conductivities than templated mesoporous silica thin films. Indeed, aerogels and xerogels had porosities varying from 25% or 90% and thermal conductivities from 0.05 to 1.02 W/mK. Note that in the above mentioned studies, porosity was often estimated from ellipsometry measurements of the effective index of refraction based on some effective medium approximation. For example, Tsui *et al.*[2] as well as Jain *et al.*[13] estimated the porosity using the parallel model[37] which underestimates the actual porosity for a given effective index of refraction.[38] Moreover, thermal conductivity measurements

reported for templated mesoporous silica thin films were performed on a total of three different films with porosities of 30% and 52% and thermal conductivity of 0.15–0.21 W/m K. Unfortunately, the pore shape, size, and spatial arrangements were unspecified.[9,24]

The goal of this study is to systematically investigate the effect of film thickness, pore geometry, pore size, and wall thickness on thermal conductivity of templated mesoporous silica thin films with monodisperse and highly ordered pores. It reports the cross-plane thermal conductivity of fully characterized cubic and hexagonal mesoporous amorphous silica thin films at room temperature for film thicknesses ranging from 85 to 540 nm, pore diameter from 3 to 18 nm, and porosity from 21% to 48%.

III. METHOD AND EXPERIMENTS

A. Sample film preparation

In the present study, highly ordered cubic and hexagonal mesoporous silica thin films with open pores were synthesized based on the calcination of self-assembled surfactant/silica or polymer/silica composites.[20] Three different types of polymer or surfactants were used, namely, polyoxyethylene (10) stearyl ether (Brij76), poly(ethylene oxide)-block-poly(propylene oxide)-block-poly(ethylene oxide) triblock copolymer ($EO_{20}PO_{70}EO_{20}$ or P123), and poly(ethylene-co-butylene)$_{89}$-b-poly(ethyleneoxide)$_{79}$ (KLE).[39] These were used to prepare open pores films with different pore sizes and interpore spacings through evaporation-induced self-assembly. Hexagonal mesoporous silica films were obtained at high surfactant concentrations, while the spherical pores arranged in a cubic structure were obtained with lower concentrations. Pores in hexagonal films were cylindrical and located at the center and apexes of hexagons when considering a transversal cut. Synthesis of the cubic mesoporous silica thin films using Brij76, P123, and KLE was based on methods developed by Jung and Park,[40] Alberius *et al.*,[19] and Smarsly and Antonietti,[41] respectively. Hexagonal mesoporous silica thin films were synthesized with P123 following the method described by Zhao *et al.*[42]

Synthesis of the cubic mesoporous silica framework using Brij76 was accomplished using a mixture of Brij76, ethanol (EtOH), 0.01*M* hydrochloric acid (HCl), and tetraethyl orthosilicate (TEOS) in the by mass ratios Brij76:EtOH:HCl:TEOS=0.17:4.42:0.43:1. A silica solution was made with 0.1 g *p*H 2.6 of HCl, 1 g of TEOS, and 0.84 g of EtOH. Solution was stirred in 60 °C water bath for 90 min. A polymer solution was then made with 3.58 g of EtOH, 0.34 g of 0.142*M* HCl, and 0.17 g of Brij 76. Solutions were mixed and stirred for 1 day. Finally films were dip coated from the solution, in 25%–30% relative humidity, and withdrawn at 0.2–2 cm/min. Calcination was followed with a heat ramp to 60 °C at 0.3 °C/min, a hold of 4 h, then another ramp to 450 °C, held also for 4 h. The process was completed by a 1 °C/min cool down ramp to 25 °C. The heating ramps were performed under inert nitrogen atmosphere.

Synthesis of the cubic mesoporous silica framework using P123 was accomplished using a mixture of P123, EtOH, 0.01*M* HCl, and TEOS in the by mass ratios P123:EtOH:HCl:TEOS=0.75:8.91:2.41:4.65. First, the P123 was dissolved in 3.57 g of EtOH and stirred for 30 min. Second, the HCl and TEOS were mixed with 5.36 g of EtOH and stirred for 20 min. Both solutions were combined and refrigerated for 10 min at 15 °C. The solution had to be used within the next hour for optimal results. The withdrawal rate was 2 cm/min at a stable 50% relative humidity. Postprocessing consisted in 1 day aging at 90% relative humidity followed by 1 day at 60 °C and calcination. For calcination, samples were heated up to 450 °C with a 4 h of soak time through a 1 °C/min ramp. The calcination process was then completed by a 1 °C/min cool down ramp to 25 °C both under inert nitrogen atmosphere.

Synthesis of the cubic mesoporous silica framework using KLE was accomplished using a mixture of KLE, EtOH, 0.01*M* HCl, and TEOS in the by mass ratios KLE:EtOH:HCl:TEOS=0.23:2:10:1. First, 0.07 g of KLE were dissolved in 2 ml of EtOH while 0.6 g of TEOS and 0.3 g of 0.01*M* HCl were mixed with 2 ml of EtOH in a separate container. Solutions were combined and stirred for 1 h. The solution was then left to age for 1 day. Films were dip coated from the aged solution onto silicon wafers in a humidity controlled chamber set to 30% relative humidity. The withdrawal rate was 2 cm/min. The films were dried overnight, then heated to 60 °C for 24 h and then calcined identically to the P123 films.

Synthesis of the hexagonal mesoporous silica framework using P123 was accomplished using a mixture of P123, EtOH, 0.01*M* HCl, and TEOS in the by mass ratios KLE:EtOH:HCl:TEOS=0.54:10:1.2:1.66. First, the P123 was dissolved in 5 g of EtOH and stirred for 30 min. Second, the HCl and TEOS were mixed with 5.36 g of EtOH and stirred for 20 min. Both solutions were then combined and aged for 3 days at room temperature. The withdrawal rate varied from 0.2 to 2 cm/min at a stable 50% relative humidity. Postprocessing consisted in 1 day of 90% room humidity aging followed by 1 day at 60 °C and then calcination as for the cubic P123 films.

B. Film characterization

Film characterization was performed using (i) one-dimensional small angle X-ray diffraction (1D-XRD), (ii) two dimensional small angles X-ray scattering (2D-SAXS), and (iii) scanning electron microscopy (SEM) measurements. 1D-XRD measurements were performed for every sample with a Panalytical X'Pert PRO diffractometer. 2D-SAXS was collected for a representative set of samples on beam lines 1–4 at the Stanford Synchrotron Radiation Laboratory. SEM images were obtained using a JEOL 6700F. 1D-XRD gave vertical repeat distance between the (111) oriented planes of the cubic films and the (10) oriented planes of the hexagonal films.

Figure 1(a) shows typical normalized 1D-XRD intensity measurements for the Brij 76 cubic, P123 cubic, KLE cubic, and P123 hexagonal mesoporous SiO_2 films. It indicates that the films are highly ordered with vertical spacings equal to 3.4, 6.8, 10.6, and 7.2 nm, respectively. Figures 1(b) and 1(c)

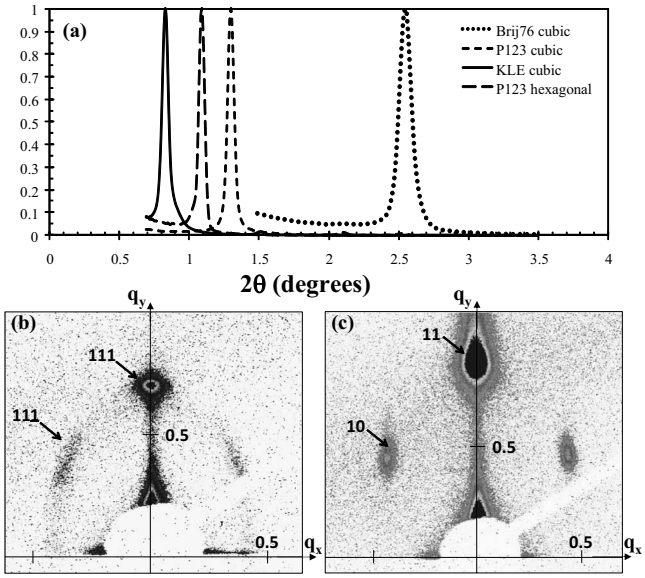

FIG. 1. (a) Normalized 1D-XRD intensity measurements for mesoporous SiO_2 thin films synthesized with Brij76 (cubic), P123 (cubic and hexagonal), and KLE (cubic); (b) 2D-SAXS patterns of a P123 cubic; and (c) a P123 hexagonal mesoporous silica thin film.

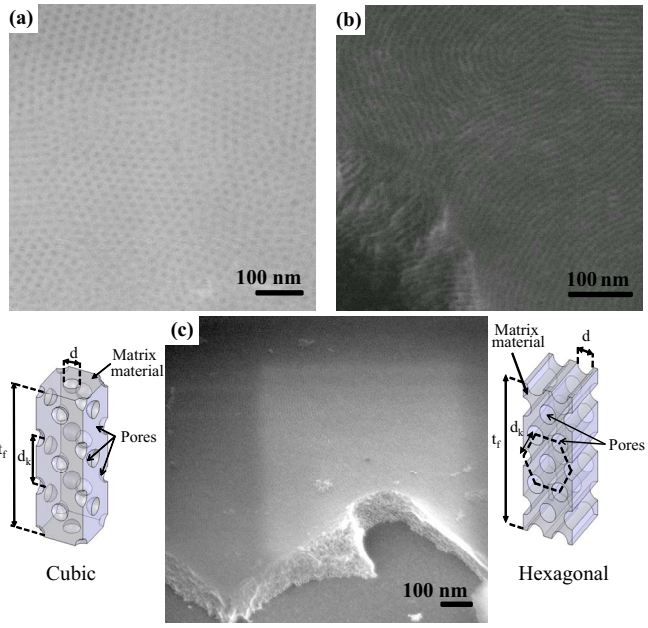

FIG. 2. (Color online) SEM picture of (a) a KLE cubic and (b) a P123 hexagonal mesoporous silica thin film. (c) Zoomed out SEM picture of a P123 hexagonal mesoporous silica thin film on top of a silicon substrate.

show typical 2D-SAXS patterns of P123 cubic and hexagonal mesoporous silica thin films. The scattering vector q is given in nm^{-1} and defined as $q=2\pi/d_{spacing}$, where $d_{spacing}$ designates the spacing between two scattering planes. They are used to estimate the original spacing between (111) planes and the vertical contraction due to silica condensation and template removal. This is achieved by assuming that contraction takes place only in the vertical direction and by comparing the (111) and $(11\bar{1})$ spacings. Original (111) spacing prior to contraction were found to be 12.4, 20.8, and 13.6 nm for P123 cubic, KLE cubic, and P123 hexagonal mesoporous films, respectively. The ratio between the vertical spacings after and before calcination ranged from 0.4 to 0.6. However, 2D-SAXS measurements of Brij76 cubic films, whose original (111) spacing was expected to be around 5.5 nm, did not provide satisfactory measurements.

Figures 2(a) and 2(b) show SEM images of KLE cubic and P123 hexagonal mesoporous films. These confirm the highly ordered structure of the films found with 1D-XRD and 2D-SAXS measurements. In addition, SEM images were used to estimate the wall thickness t_{wall} separating two adjacent pores and the horizontal center to center pore distance. The porosity of the films consists of (i) the primary mesoporosity corresponding to the volume fraction occupied by the quasispherical pores and of (ii) the microporosity corresponding to the volume fraction occupied by the "necks" connecting the pores. Samples primary mesoporosity was estimated from the measured pore diameters and lattice spacings. On the other hand, cubic films microporosity could be evaluated by comparing the estimated mesoporosity with the total porosity measured by Fattakhova-Rohlfing *et al.*[39] using adsorption isotherms of Kr at 77 K on similar titania samples. Cubic films microporosity was estimated to be around 12%–20% of the mesoporosity which is also in good agreement with microporosities reported in Ref. 43 for cubic silica films. Hexagonal film microporosity, however, is expected to be much smaller since a geometric model of cylinders should better capture the major porosity of a hexagonal material.

Cubic mesoporous thin films consisted of spherical pores of diameter d organized in a face cubic centered structure of lattice parameter d_k [Fig. 2(a)]. The cubic SiO_2 films synthesized from Brij76, P123, and KLE surfactants exhibited pore diameters d between 3 and 5, 8 and 10, and 15 and 18 nm, respectively. The wall thicknesses t_{wall} ranged from 2 to 3, 3 to 5, and 10 to 12 nm while the associated lattice parameters d_k varied between 7 and 11, 15 and 21, and 35 and 42 nm, respectively. The film mesoporosity is expressed as $f_v=2\pi d^3/3d_k^3$ and the average porosity was found to be 22%, 25%, and $28\pm5\%$ for films made from Brij76, P123, and KLE, respectively. There was a $\pm5\%$ uncertainty associated with the porosity measurements due to the 1 nm precision on distances measured with the SEM and the approximation in calculating the microporosity contribution. These results were in good agreement with those reported by Kitazawa *et al.*[44] for similar P123 cubic mesoporous silica thin films and obtained using ellipsometry.

The hexagonal films consisted of a honeycomb pattern of cylindrical pores of diameter d, with the unique hexagonal axis oriented parallel to the substrate [Fig. 2(b)]. The lattice parameter d_k and the wall thickness t_{wall} ranged from 11 to 15 and from 3 to 5 nm, respectively. The pore diameter varied from 7 to 10 nm. The mesoporosity of hexagonal mesoporous films is given by $f_v=\pi d^2/2\sqrt{3}d_k^2$ and porosity was found to be $44\pm5\%$. These results were in good agreement with those reported by Dourdain *et al.*[45] for similar P123 hexagonal mesoporous silica thin films and measured using X-ray reflectivity and grazing incident small angle X-ray scattering (GISAXS).

Spectral normal reflectance measurements were performed for wavelength between 400 and 900 nm. The effec-

tive refractive index n_f and film thickness t_f of all samples were retrieved by inverse method using the genetic algorithm PIKAIA[46] that minimizes the root mean square (rms) of the relative error between experimental and theoretical spectral reflectance δR defined as

$$\delta R^2 = \frac{1}{N}\sum_{i=1}^{N}\left[\frac{R_{\text{th}}(\lambda_i) - R_{\text{expt}}(\lambda_i)}{R_{\text{expt}}(\lambda_i)}\right]^2. \quad (1)$$

The thickness of the synthesized mesoporous thin films ranged from 85 to 540 nm. The film porosity was also deduced from the retrieved effective index of refraction based on effective medium approximation such as the Maxwell–Garnett, Lorentz–Lorenz, Bruggeman, the parallel, series, and the volume average theory models.[47,48] Note that for mesoporous silica, the porosity predicted by these models falls within 15% of each other. In addition, the retrieved porosity using the Maxwell–Garnett model, validated by Hutchinson *et al.*,[38] were in good agreement with the SEM/XRD measurements for most films. The study showed, however, that porosities retrieved from the optical measurements sometimes disagreed with expected values from the fabrication process and from SEM/XRD measurements. In particular, six cubic samples made from Brij76 and P123 surfactants showed unrealistically low porosities. This could be attributed to water remaining within the pores even after dehydration. Indeed, the brij76 samples had pores less than 4 nm in diameter and the three cubic P123 samples that showed deviations also showed large lattice contractions normal to the substrate after calcination making the water removal difficult. This and the approximation made by using effective medium approximations show some limits to measuring porosity using optical methods, particularly for small pores materials. Dourdain *et al.*[45] also discussed the difficulty to precisely retrieve porosity values using conventional methods such as ellipsometry or gas adsorption and proposes the use of X-ray reflectivity GISAXS patterns for this purpose. SEM pictures combined with 2D-XRD measurements give a more reliable but potentially less precise information than optical measurements.

C. Principles of the 3ω method

The use of conventional methods to measure the thermal conductivity of thin films can lead to significant errors.[49,50] Previous studies have shown that the 3ω method[36,51] is a reliable method which has been used extensively for measuring thermal conductivity of dielectric thin films. In this method, a highly conductive metallic wire, serving as both a thermometer and a line heat source, is patterned on top of the dielectric film of interest.[51] The fluctuations in electrical resistance of the wire are driven by the sample surface temperature changes with amplitude $\Delta T_{\text{expt}}(\omega)$. The thermal conductivity of the thin film is retrieved by analyzing the harmonic response of the temperature fluctuations of the sample. The film is considered to be thermally thin when the film thickness t_f is much smaller than the thermal penetration depth $D_f = \sqrt{\alpha_f/4\pi\omega}$, where α_f and 2ω are the film's thermal diffusivity and the temperature oscillation frequency, respectively.[51] In other words, if $t_f \ll D_f$, the wavelength of the diffusive thermal wave is larger than the film thickness. For example, the thermal penetration depth D_f of a thermally grown SiO_2 film is estimated to be 2.57 μm at frequency ω of 10 kHz using the value of thermal diffusivity of bulk fused silica glass at room temperature ($\alpha_f = 9\times10^{-7}$ m^2/s).[52]

The sample surface temperature $\Delta T_{\text{expt}}(\omega)$ is determined by measuring the third-harmonic voltage drop across the metal wire $V_{3\omega}$ and is expressed as[53]

$$\Delta T_{\text{expt}}(\omega) = \frac{2V_{3\omega}}{\gamma V}, \quad (2)$$

where $\gamma = (dR_e/dT)/R_{e,0}$ is the temperature resistance coefficient of the patterned metal strip and $R_{e,0}$ is its resistance at room temperature; V is the voltage drop across the metal line at ω. All reported voltages are rms voltages. The theoretical amplitude of the temperature oscillation of the substrate, $\Delta T_w^*(\omega)$, can be calculated from the heat diffusion equation for the instantaneous line source. For cases when the thermal penetration depth within the wafer D_w is much larger than the heater's width b (i.e., $D_w \gg b$), $\Delta T_w^*(\omega)$ in complex notation is given by[53]

$$\Delta T_w^*(\omega) = \frac{P}{\pi L k_w}\left\{\frac{1}{2}\ln\left(\frac{D_w}{b^2}\right) + 0.932 - \frac{1}{2}\ln(2\omega) - \frac{i\pi}{4}\right\}, \quad (3)$$

where $P = VR_0$ is the power dissipated by the metal strip, L is the length of the metal strip, and k_w is the thermal conductivity of the substrate. The thermal conductivity k_w can then be calculated from the slope of the semilogarithmic plot of $\Delta T_{\text{expt}}(\omega)$ versus $\ln(\omega)$ measured for the bare silicon wafer.

Unfortunately, the photolithographic process to pattern the metallic wire involves some strongly basic chemicals which can damage the mesoporous silica thin films. Therefore, a plasma enhanced chemical vapor deposition (PECVD) silicon nitride layer with thickness t_{SiN} (less than 500 nm thick) was deposited between the film and the metallic heater as a protective cap layer. The deposition was very conformal and provided good step coverage to prevent chemicals from coming in contact with the mesoporous film. The effective thermal conductivity of the silicon nitride layer, denoted by k_{SiN}, was also measured separately for each sample and found to be equal to 1.2 ± 0.4 W/m K. This was achieved by measuring the thermal conductivity of an identical silicon nitride layer deposed on a bare silicon wafer placed within the same PECVD chamber as the mesoporous silica thin films. This value also accounts for the additional contact resistance between the silicon nitride layer and the layer below. The total thermal resistance of the multilayered structure r_{tot} is thus given by

$$r_{\text{tot}} = r_f + r_{\text{SiN}}, \quad (4)$$

where $r_{\text{tot}} = t_{\text{tot}}/k_{\text{tot}}$, $r_f = t_f/k_f$, and $r_{\text{SiN}} = t_{\text{SiN}}/k_{\text{SiN}}$.

For the multilayered structure of interest, $\Delta T_{\text{expt}}(\omega)$ corresponds to the sum of the in-phase component $\Delta T_w(\omega)$ (i.e., the real part) of the temperature oscillation of the substrate $\Delta T_w^*(\omega)$ and the temperature response of the superimposed

SiN and SiO_2 thin films denoted by ΔT_{tot}.[54] The latter is independent of frequency and is expressed as[36]

$$\Delta T_{tot} = \frac{Pt_{tot}}{2bLk_{tot}} = \Delta T_{expt}(\omega) - \Delta T_w(\omega). \quad (5)$$

Here t_{tot} is the total thickness equal to $t_f + t_{SiN}$ and k_{tot} is the corresponding thermal conductivity. $\Delta T_{expt}(\omega)$ was measured experimentally using Eq. (2). The total thermal conductivity of the multilayered structure k_{tot} was then determined from

$$k_{tot} = \frac{Pt_{tot}}{2bL[\Delta T_{expt}(\omega) - \Delta T_w(\omega)]}. \quad (6)$$

Finally, the effective thermal conductivity of the mesoporous silica thin film was computed according to

$$k_f = t_f \left[\frac{t_{tot}}{k_{tot}} - \frac{t_{SiN}}{k_{SiN}} \right]^{-1}. \quad (7)$$

D. Experimental apparatus

The experimental setup for the 3ω method consisted of (1) a lock-in amplifier (Stanford research system, SR830), (2) a custom designed probe-card by Alpha-Probes Inc., (3) a metal wire patterned on top of the mesoporous silica thin films, and (4) an electrical circuit. The lock-in amplifier served as (i) a multimeter to measure the voltage drop across the metal wire, (ii) a function generator to generate a sinusoidal current, and (iii) a power supply to supply a bias voltage for the differential amplifiers (Analog devices, AD524) used in the electrical circuit. The probe card was used to establish electrical contacts on four pads of the metal wire.

A wire made of 100 nm of aluminum (Al) on top of 10 nm of chromium (Cr) [Cr (10 nm)/Al (100 nm)], which functioned as both heater and thermometer, was patterned on each sample surface and fabricated by photolithography, e-beam evaporation, and finally lift-off. The length (L) and width ($2b$) of the metal wire were 1 mm and 30 μm, respectively. Theoretically a metal wire width of 30 μm should be too wide to satisfy the relationship $D_w \gg b$ for frequencies lower than 1000 Hz and the conditions of validity of Eq. (3). Actual experimental results however, were not affected and did not differ with those obtained from 5 μm wide heaters. Because the metal patterning process is easier and more accurate for wider patterns, the study was conducted with 30 μm wide metal strips. Figure 3(a) shows the custom designed probe card and the metal wire used in the actual experiment along with the location of the four probes numbered 1–4.

Figure 3(b) shows the electrical circuit used to implement the 3ω method along with the nodes associated with the four pads shown in Fig. 3(a). The electrical circuit was designed to measure the third-harmonic component of the voltage drop $V_{3\omega}$ across the metal wire and to achieve maximum signal to noise ratio. Moreover, it is essential to have a reference resistor whose resistance does not vary since the 3ω method relies on measuring small voltage fluctuations across the metal wire. In the first harmonic mode, the A-B signal

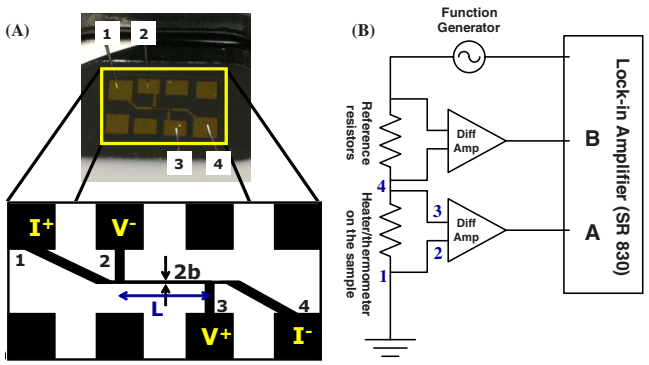

FIG. 3. (Color online) (a) Schematic and photograph of the metallic heater and contact pads and (b) electrical circuit used for the 3ω method (inspired from Ref. 36).

[Fig. 3(b)] should be set as close to 0 V as possible, typically below 0.5 mV, by adjusting the reference resistance to match the patterned wire resistance.

E. Experimental procedure

All the samples were dehydrated for a minimum of 24 h at 160 °C on a hotplate before performing both the reflectance and thermal conductivity measurements. The electrical resistance $R_{e,0}$ and the coefficient $\gamma = (dR_e/dT)/R_{e,0}$ of the metal wire were determined by measuring the electrical resistance at seven different temperatures between 20 and 60 °C achieved by heating the metal with a silicone rubber heating tape (Briskheat, XtreamFLEX™ BS0) placed underneath the sample. The third-harmonic voltage drop across the metal wire $V_{3\omega}$ was measured at 16 different frequencies between 70 and 7 kHz. The relevant frequency range was mostly between 100 and 1000 Hz by virtue of assumptions made to derive Eq. (3).

F. Validation

The experimental apparatus and procedure as well as the associated data analysis were validated by measuring the thermal conductivity of a silicon wafer and of high quality thermal oxide thin films. First, the thermal conductivity of a (100) p-type silicon wafer with doping concentration of 2×10^{15} cm^{-3} patterned with an Al metallic heater was measured to be 137.5 ± 9.6 W/m K at 297 K. This falls within 8.3% of the reported value of 150 W/m K.[55]

Similarly, the thermal conductivity of high quality thermal oxide films with thicknesses equal to 105, 279, 310, and 511 nm was measured at room temperature as 0.76 ± 0.11, 0.97 ± 0.11, 1.05 ± 0.07, and 1.25 ± 0.17 W/m K, respectively. These values were obtained by averaging eight repeated measurements for each sample and the experimental uncertainty was estimated with 95% confidence interval. These measurements were compared to predictions of the thermal conductivity model developed by Lee and Cahill[54] and expressed as

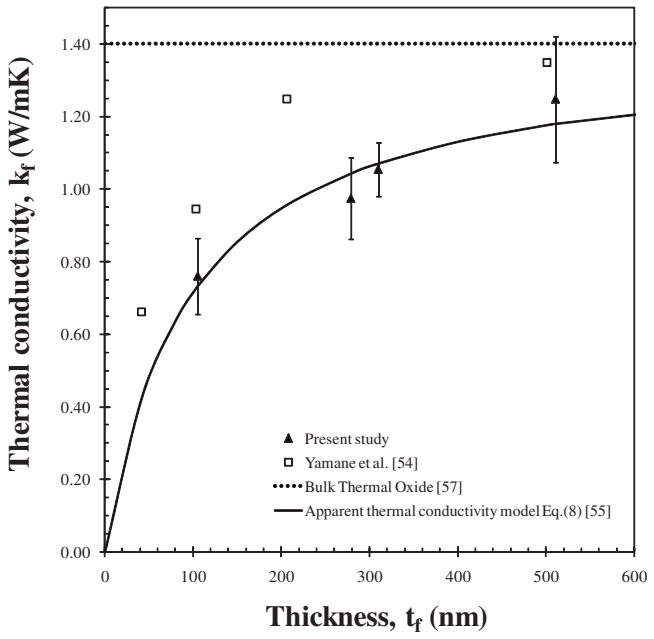

FIG. 4. Measured thermal conductivity of high quality thermal oxide dense films as a function of film thickness along with previously reported data (Refs. 53, 54, and 56).

$$k_f = \frac{k_i}{1 + k_i r_c / t_f}, \tag{8}$$

where k_i is the intrinsic thermal conductivity which is independent of thickness. Equation (8) as well as the measured thermal conductivity, k_f, account for the contribution of the contact thermal resistance r_c due to the interfaces between (i) the dielectric film and the silicon substrate and (ii) between the metallic heater and the dielectric film. The value of k_i used in Eq. (8) was reported in literature as 1.4 W/m K (Ref. 56) and a value of $r_c = 6.96 \times 10^{-8}$ m^2 K/W was found to provide the best fit to our experimental data. This value is in good agreement with the values of 2.00×10^{-8} and 3.40×10^{-8} m^2 K/W reported for PECVD silicon dioxide[54] and for thermal oxide,[53] respectively, measured with gold heaters. Note that the value of r_c depends on the metal used and on surface roughness among other parameters.

Figure 4 compares the thermal conductivity measurements for different SiO_2 film thicknesses obtained in the present study with predictions from Eq. (8) and experimental data reported by Yamane *et al.*[53] The thermal conductivity obtained in the present study falls within 24% of previously reported data for thickness ranging from 50 to 500 nm.[53] Differences can be attributed (i) to the use of aluminum instead of gold for the metallic wire heater and (ii) to possible variations in the contact quality due to differences in deposition conditions for both the films and the heaters. Overall, the experimental setup and the associated analysis have been implemented successfully and can be utilized to measure the thermal conductivity of the synthesized mesoporous silica thin films.

IV. RESULTS AND DISCUSSION

The cross-plane thermal conductivity of the highly ordered mesoporous amorphous silica thin films was measured with the previously described 3ω method. The film thickness t_f varied from 85 to 540 nm. The values of P/L and γ were measured before each test for each sample and were found to be 35 ± 3 W/m and $(2.3 \pm 0.3) \times 10^{-3}$ K^{-1}, respectively. The amplitude of the temperature oscillations of the multilayered structure ΔT_{tot} was found to be independent of frequency as previously discussed. The thermal conductivity of each mesoporous silica film was measured more than eight times and averaged. The experimental uncertainty associated with the thermal conductivity of the mesoporous thin films was estimated to be less than 30% with 95% confidence interval. Table I summarizes the measured thermal conductivity results along with the thickness, porosity, pore size, and wall thickness of the synthesized cubic and hexagonal mesoporous thin films.

A. Effect of film thickness

This section investigates possible dependency of thermal conductivity with respect to mesoporous film thickness similar to what was observed with dense thermal oxide thin films

TABLE I. Thermal conductivity of the synthesized cubic and hexagonal mesoporous amorphous silica thin films.

Sample No.	Structure	Surfactant	Porosity f_v (±5%)	Film thickness t_f (nm)	Pore diameter d (nm)	Wall thickness t_{wall} (nm)	Conductivity k_f (W/m K)
1	Hexagonal	P123	46%	320	7–10	3–5	0.18 ± 0.02
2	Hexagonal	P123	48%	160	7–10	3–5	0.18 ± 0.01
3	Hexagonal	P123	40%	300	7–10	3–5	0.22 ± 0.01
4	Hexagonal	P123	43%	540	7–10	3–5	0.20 ± 0.01
5	Hexagonal	P123	45%	130	7–10	3–5	0.18 ± 0.01
6	Cubic	Brij76	21%	155	3–5	2–3	0.30 ± 0.04
7	Cubic	Brij76	23%	150	3–5	2–3	0.29 ± 0.02
8	Cubic	Brij76	23%	170	3–5	2–3	0.34 ± 0.03
9	Cubic	P123	29%	185	8–10	3–5	0.28 ± 0.03
10	Cubic	P123	23%	200	8–10	3–5	0.38 ± 0.02
11	Cubic	P123	26%	85	8–10	3–5	0.27 ± 0.01
12	Cubic	P123	25%	80	8–10	3–5	0.27 ± 0.01
13	Cubic	KLE	27%	300	15–18	10–12	0.35 ± 0.01
14	Cubic	KLE	30%	130	15–18	10–12	0.32 ± 0.04

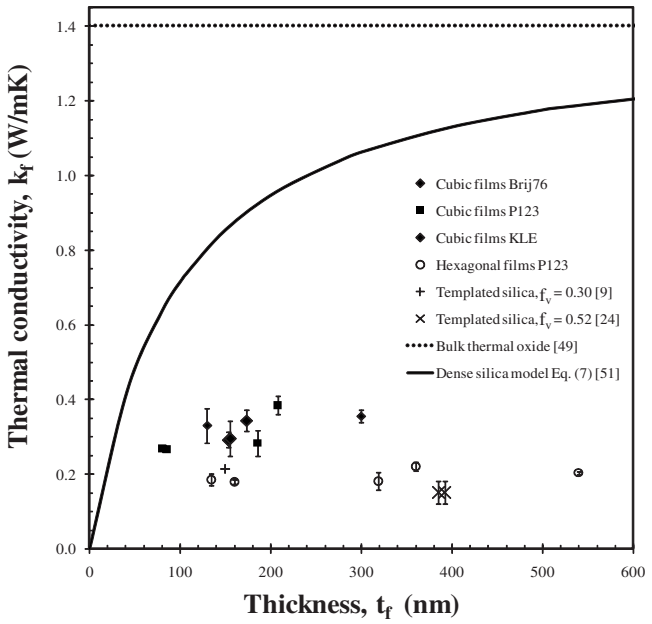

FIG. 5. Comparison between the measured cross-plane thermal conductivity of cubic and hexagonal mesoporous silica thin films at room temperature as a function of film thickness along with previously reported data (Refs. 9 and 24).

(Fig. 4). Five P123 hexagonal films (samples 1–5) were synthesized with different thicknesses, but identical porosities (f_v=45%), pore diameters (d=8 nm), pore arrangements (hexagonal), and wall thicknesses (t_{wall}=4 nm). In this way only film thickness could influence the measurements. Figure 5 shows the thermal conductivity of the hexagonal mesoporous silica thin films at room temperature as a function of film thickness. It establishes that the cross-plane thermal conductivity of the hexagonal mesoporous silica thin film (i) is three to five times lower than that of dense silica thin films of the same thickness and (ii) does not vary with film thickness. This result was also observed with cubic films made with different surfactants, as illustrated in Fig. 5.

Because of the significant atomic scale disorder of amorphous silica, phonons cannot be well defined.[29] The vibrational modes responsible for heat conduction do not propagate like phonons in crystals.[57] Heat transfer can either be analyzed in terms of energy hopping between localized, nonpropagating, vibrational modes,[57,58] or in terms of "diffusion" of energy between extended non propagating vibrational modes.[59] The amplitude of those vibrational modes is of the same order of magnitude as the interatomic distances in the silica films and the intrinsic thermal conductivity of the film k_i is, therefore, independent of film thickness.

The effective thermal conductivity expressed in Eq. (8) depends on the film thickness t_f through the effect of the contact thermal resistances between the films and both the heater and the wafer denoted by r_c. The value of r_c for dense silica thin films is of the same order of magnitude as the film total thermal resistance given by t_f/k_i. However, for mesoporous silica thin films, the effect of interfacial thermal resistance r_c is negligible since its magnitude is about ten times smaller than the effective thermal resistance of the mesoporous silica thin films equal to t_f/k_i. Indeed, the interfacial thermal resistance values range between 2.0×10^{-8} m^2 K/W (Ref. 54) and 7.0×10^{-8} m^2 K/W in the present study while the effective thermal resistance of the hexagonal mesoporous silica thin films fall between 5.0×10^{-7} and 2.5×10^{-6} m^2 K/W. In other words, referring to Eq. (8), $k_i r_c/t_f \approx 1$ for thermal oxide films while $k_i r_c/t_f \ll 1$ for mesoporous silica thin films. Thus in the latter case and according to Eq. (8): $k_f \approx k_i$.

Experimental results establish that the intrinsic thermal conductivity of the mesoporous silica thin films k_i is lower than that of dense silica thin films. This can be attributed to a purely geometrical effect resulting from the reduction in the cross section through which the heat diffuses in the mesoporous silica.[28] The film thickness can, nevertheless, be expected to have some influence on thermal conductivity at lower porosities and/or very small thicknesses.

B. Effect of porosity

Porosity of mesoporous thin films varied between 21% and 30% for cubic films and between 40% and 48% for hexagonal films. As the heat is carried by very localized nonpropagating vibrational modes whose coherent lengths remain much smaller than wall thicknesses, effective medium approximation can be used to model the effect of porosity.[32] Thus, experimental results were compared with various models including the parallel model, series model, dilute particle model, dilute fluid model,[52] as well as the porosity weighted simple medium (PWSM) model and porosity weighted dilute medium (PWDM) model.[14] These models attempt to represent intrinsic thermal conductivity variations of the material and do not account for interfacial thermal resistance.

The PWSM model is given by[14]

$$k_f = k_i \frac{f_v k_a + (1-f_v)k_i}{k_i}[1-(f_v)^x] + k_a \frac{k_i}{f_v k_i + (1-f_v)k_a}(f_v)^x, \quad (9)$$

with f_v as defined in Sec. III. Here, k_i is the thermal conductivity of bulk SiO_2 matrix equal to 1.40 W/m K (Ref. 56) and k_a is the thermal conductivity of air equal to 0.0257 W/m K, both at room temperature. The semiempirical fitting parameter x ranges from zero to infinity and accounts for the cumulative effects of pore shape, pore size, and other parameters on thermal conductivity.[14] Similarly, the PWDM model is given by[14]

$$k_f = k_i \frac{2(1-f_v)k_i + (1-2f_v)k_a}{(2+f_v)k_i + (1-f_v)k_a}[1-(f_v)^x] + k_a \frac{(3-2f_v)k_i + 2f_v k_a}{f_v k_i + (3-f_v)k_a}(f_v)^x. \quad (10)$$

The PWSM model is a weighted sum of the parallel and the series model while the PWDM is a weighted sum of the dilute fluid and dilute particle models. For x=0, the PWSM and PWDM models correspond to the series and dilute particle models, respectively. On the other hand, when x tends to infinity, they correspond to the parallel and the dilute fluid

models, respectively. The physical meaning of these two semiempirical was provided by Hu *et al.*[14]

Alternatively, the coherent potential (CP) approximation also known as the symmetric Bruggeman theory[60] was independently derived by Landauer[61] to model the electrical conductivity of composite materials with spherical inclusions. Cahill and co-workers used it to predict the thermal conductivity of porous Vycor glass[51] and XLK.[32] This model simplifies to

$$k_f = k_i(1 - 1.5f_v). \tag{11}$$

It predicted the overall trend of measured thermal conductivity as a function of temperature of the porous Vycor glass with porosity approximately equal to 30% and pores size around 10 nm between 30 and 300 K.[28] However, careful analysis shows that it systematically overpredicts the thermal conductivity of the Vycor glass for all temperatures with nearly a factor 2.0 at room temperature (Ref. 62, Fig. 3).

Moreover, Costescu *et al.*[32] compared experimental data for XLK, aerogels, xerogels, Vycor, and dense SiO_2 with the Clausius–Mossoti (CM) approximation and the differential-effective medium (DEM) theory given by[32]

$$k_f = k_i \frac{2(1 - f_v)}{2 - f_v}, \quad \text{CM approximation}, \tag{12}$$

$$k_f = k_i(1 - f_v)^{3/2}, \quad \text{DEM theory}, \tag{13}$$

where the ratio of atomic density of the porous films and the matrix is assumed to be equal to the density ratio $\rho_f/\rho_i = 1 - f_v$. However, careful analysis shows that they do not precisely predict the measured thermal conductivities.

A single model may not be able to correctly predict the entire experimental data given the different morphologies and pore sizes as well as the experimental uncertainties in measuring both porosity and thermal conductivity. Thus, it is more appropriate to predict an upper and lower bounds for the film effective thermal conductivity. The parallel and series models constitute two such bounds.[63] However, the difference between these two models is large and models providing narrower bounds are desirable.[63] The dilute fluid and dilute particle models were considered as bounds for the thermal conductivity of silica matrix with spherical pores.[14] Similarly, the effective thermal conductivity of the mesoporous structure is expected to lie between the PWSM and PWDM models.[14]

Figure 6 shows the measured thermal conductivity of all synthesized films as a function of porosity along with predictions of the different effective medium approximations previously discussed. It also includes the experimental data reported by Delan *et al.*,[24] Tsui *et al.*,[2] and Choi *et al.*[9] for mesoporous silica thin films with various porosities. Experimental data from the present study fall between the PWSM and PWDM models for a value of $x = 0.17$ fitted by least square method using all data obtained in this study. The analysis also shows that the other models underpredict (series model, dilute particle model) or overpredict (dilute fluid model, parallel model, CP, CM, and DEM models) the measured thermal conductivity.

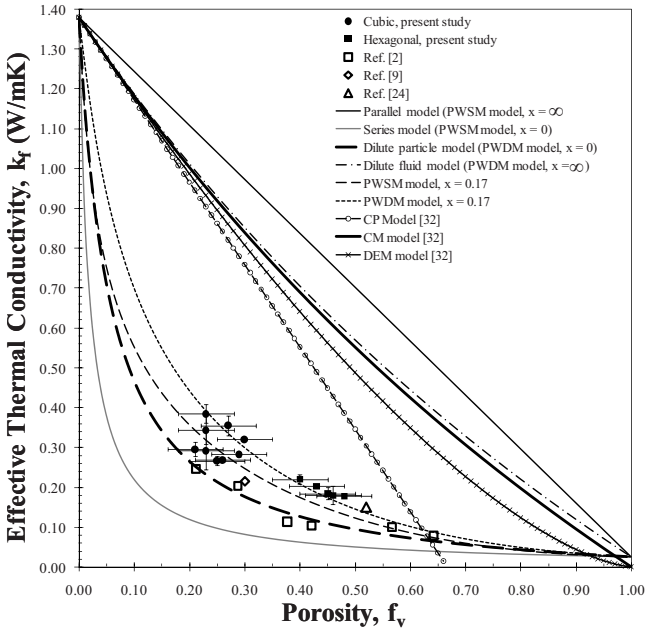

FIG. 6. Comparison of the measured cross-plane thermal conductivity with the previously proposed nine models (Refs. 14, 32, and 52) and previously reported data for templated mesoporous (Refs. 9 and 24) and selected porous (Ref. 2) silica films. The experimental data were best fitted between the PWSM [Eq. (9)] and PWDM [Eq. (10)] models for $x = 0.17$ (Refs. 2, 9, and 24).

Note that the lower the porosity, the higher the effective thermal conductivity of the mesoporous thin film, and the more it may be affected by film thickness. However, thickness was shown to have a negligible effect for porosities considered in this study.

C. Effects of pore diameter and wall thickness

All cubic mesoporous silica films were amorphous and exhibited similar porosities in the range between 21% and 30%. These films featured very different pore diameters and wall thicknesses (see Table I). However, despite this fact, their thermal conductivity varied between 0.27 ± 0.01 and 0.38 ± 0.02 W/m K with an average value of 0.3 W/m K. This is almost five times lower than the thermal conductivity of bulk SiO_2, estimated at 1.40 W/m K.[56] However, somewhat surprisingly, experimental results established that pore diameter and wall thickness do not seem to significantly affect the effective thermal conductivity. This result can be attributed to the fact that the amplitude of the localized vibrational modes responsible for heat transfer in amorphous silica is ten times smaller than the thickness of the thinnest walls. The wall thickness is expected to have an effect at very low temperatures. Indeed, at low temperatures, the energy is carried by long wavelength phonons[64] with longer mean free paths which become comparable or larger than the wall thickness.

Finally, experimental measurements showed little influence of morphology on thermal conductivity at room temperature. Differences between cubic and hexagonal mesoporous thin films can be dominantly attributed to differences in porosities and data for both morphologies could be fit to the same model (Fig. 6). All hexagonal films had nearly identical

wall thicknesses and show a much tighter correlation between thermal conductivity and porosity than the cubic films. Cubic thin films are expected to have the same in-plane and cross-plane thermal conductivities due to their isotropic structure. The same results are expected for hexagonal films. Indeed, as indicated in Fig. 2(b), cylindrical pores are aligned in domains of a few hundred of nanometers in size. These domains are randomly oriented and no anisotropy in thermal conductivity due to the pore arrangement can thus be expected beyond the scale of one domain.

V. CONCLUSION

This paper presented preparation, characterization, and cross-plane thermal conductivity measurements at room temperature of cubic and hexagonal mesoporous amorphous silica thin films with various thicknesses, pore sizes, pore shapes, and porosities. The following conclusions could be drawn.

(1) The average thermal conductivity of cubic and hexagonal mesoporous thin films with average porosity of 25% and 44% were measured as 0.30 and 0.20 W/m K, respectively. This represents a reduction by 79% and 86% of bulk dense silica thermal conductivity at room temperature, respectively.
(2) The thermal conductivity of the synthesized hexagonal mesoporous silica thin films was found independent of the film thickness ranging from 130 to 500 nm. This can be attributed to the fact that the thermal resistance of the mesoporous films is much larger than the contact resistance.
(3) The effective thermal conductivity of mesoporous SiO_2 thin films decreased with porosity and experimental data fell between the PWSM and PWDM models with $x=0.17$.
(4) Pore diameter and wall thickness did not have a significant effect on the effective thermal conductivity of the synthesized thin films.

ACKNOWLEDGMENTS

The authors thank Thomas Quickel for the 2D-SAXS measurements. This material is based upon the work supported by the National Science Foundation under Grant Nos. CTS 0449429 (L.P.) and CHE-0527015 (S.H.T) and by the Intel, NERC, and UC Discovery Program. Portions of this research were carried out at the Stanford Synchrotron Radiation Laboratory, a national user facility operated by Stanford University on behalf of the U.S. Department of Energy, Office of Basis Energy Science.

NOMENCLATURE

b	Half width of metal strip (μm)
C	Capacitance (F)
D_f	Thermal penetration depth within the film (m)
D_w	Thermal penetration depth within the wafer (m)
d	Pore diameter (m)
d_k	Lattice parameter (m)
f_v	Porosity
I	Current (A)
k	Thermal conductivity (W/m K)
L	Metal strip length (m)
P	Power dissipation (W)
r	Thermal resistance (m^2 K/W)
R	Reflectance
R_e	Electrical resistance (Ω)
t	Thickness (m)
T	Temperature (K)
V	Voltage (V)
$V_{3\omega}$	Third harmonic voltage drop (V)

Symbols

α	Thermal diffusivity (m^2/s)
γ	Thermal coefficient of resistance ($1/K$)
ε_r	Dielectric constant
ω	Frequency (Hz)
ρ	Density (kg/m^3)

Subscripts

0	Initial condition at room temperature
c	Contact interface
expt	Experimental data
f	Thin film
i	Bulk property
SiN	Silicon nitride layer
SiO_2	Silicon dioxide
th	Theoretical data
tot	Mesoporous film and SiN layer
w	Wafer
wall	Walls between adjacent pores

[1] Semiconductor Industry Association, The International Technology Roadmap for Semiconductors, 2006.
[2] B. Y. Tsui, C. C. Yang, and K. L. Fang, IEEE Trans. Electron Devices **51**, 20 (2004).
[3] K. N. Tu, J. Appl. Phys. **94**, 5451 (2003).
[4] S. Baskaran, J. Liu, K. Domansky, N. Kohler, X. Li, C. Coyle, G. E. Fryxell, S. Thevuthasan, and R. E. Williford, Adv. Mater. (Weinheim, Ger.) **12**, 291 (2000).
[5] K. R. Carter, H. J. Cha, R. A. DiPietro, C. J. Hawker, J. L. Hedrick, J. W. Labadie, J. E. McGrath, T. P. Russell, M. I. Sanchez, S. A. Swamsom, W. Volksen, and D. Y. Yoon, Materials Research Society Symposium Proceedings (Materials Research Society, Pittsburgh, PA, 1995), Vol. 381, pp. 79–92.
[6] S. M. Hong and S. S. Hwang, J. Appl. Polym. Sci. **100**, 4964 (2006).
[7] T. Brady, D. Bodas, D. Gabel, B. Griffith, T. Niemela, and D. Perchlik, Proceedings of the 2005 IEEE International Symposium on Electronics and the Environment, New Orleans, LA, 16–19 May 2005 (unpublished).
[8] C. D. Patel, The International Symposium on Micro-Mechanical Engineering, ISMME2003-K15, Tsuchiura and Tsukuba, Japan, 1–3 December 2003 (unpublished).
[9] S. G. Choi, T.-J. Ha, B.-G. Yu, S. P. Jaung, O. Kwon, and H.-H. Park, Ceram. Int. **34**, 833 (2008).
[10] M. E. Davis, Nature (London) **417**, 813 (2002).
[11] C. J. Brinker, Y. Lu, A. Sellinger, and H. Fan, Adv. Mater. (Weinheim, Ger.) **11**, 579 (1999).
[12] M. A. Einarsrud, S. Haereid, and V. Wittwer, Sol. Energy Mater. Sol. Cells **31**, 341 (1993).
[13] A. Jain, S. Rogojevic, S. Ponoth, W. N. Gill, and J. L. Plawsky, J. Appl. Phys. **91**, 3275 (2002).
[14] C. Hu, M. Morgen, P. S. Ho, A. Jain, W. N. Gill, J. L. Plawsky, and P. C. Wayner, Appl. Phys. Lett. **77**, 145 (2000).
[15] J. S. Beck, J. C. Vartuli, W. J. Roth, M. E. Leonowicz, C. T. Kresge, K. D. Schmitt, C. T. W. Chu, D. H. Olson, and E. W. Sheppard, J. Am. Chem. Soc. **114**, 10834 (1992).

[16]D. Zhao, J. Feng, Q. Huo, N. Melosh, G. H. Fredrickson, B. F. Chmelka, and G. D. Stucky, Science **279**, 548 (1998).
[17]Y. Lu, R. Ganguli, C. A. Drewien, M. T. Anderson, C. J. Brinker, W. Gong, Y. Guo, H. Soyez, B. Dunn, M. H. Huang, and J. I. Zink, Nature (London) **389**, 364 (1997).
[18]A. R. Balkenede, F. K. de Theije, and J. C. K. Kriege, Adv. Mater. (Weinheim, Ger.) **15**, 139 (2003).
[19]P. C. A. Alberius, K. L. Frindell, R. C. Hayward, E. J. Kramer, G. D. Stucky, and B. F. Chmelka, Chem. Mater. **14**, 3284 (2002).
[20]B. W. Eggiman, M. P. Tate, and H. W. Hillhouse, Chem. Mater. **18**, 723 (2006).
[21]C. Jin, S. Lin, and J. T. Wetzel, J. Electron. Mater. **30**, 284 (2001).
[22]M. R. Böhmer, A. R. Balkenende, T. N. M. Bernards, M. P. J. Peeters, M. J. van Bommel, E. P. Boonekamp, M. A. Verheijen, L. H. M. Krings, and Z. A. E. P. Vroon, *Handbook of Advanced Electronic and Photonic Materials and Devices*, Chalcogenide Glasses and Sol-Gel Materials Vol. 5 (Academic, San Diego, CA, 2001).
[23]J. L. Hedrick, R. D. Miller, C. J. Hawker, K. R. Carter, W. Volksen, D. Y. Yoon, and M. Trollsås, Adv. Mater. (Weinheim, Ger.) **10**, 1049 (1998).
[24]A. Delan, M. Rennau, S. E. Schulz, and T. Gessner, Microelectron. Eng. **70**, 280 (2003).
[25]S. V. Nitta, V. Pisupatti, A. Jain, P. C. Wayner, Jr., W. N. Gill, and J. L. Plawsky, J. Vac. Sci. Technol. B **17**, 205 (1999).
[26]H. J. Lee, C. L. Soles, D. W. Liu, B. J. Bauer, and W. L. Wu, J. Polym. Sci., Part B: Polym. Phys. **40**, 2170 (2002).
[27]P. Scheuerpflug, M. Hauck, and J. Fricke, J. Non-Cryst. Solids **145**, 196 (1992).
[28]D. G. Cahill, R. B. Stephens, R. H. Tait, S. K. Watson, and R. O. Pohl, in *Thermal Conductivity 21: Proceedings of the 21st International Thermal Conductivity Conference*, Lexington, KY, 15–18 October 1989, edited by C. J. Cremers and H. A. Fine (Springer, New York, 1990).
[29]D. G. Cahill, in *Microscale Energy Transport*, edited by C. L. Tien, A. Majumdar, and F. M. Gerner (Taylor & Francis, Washington, DC, 1997), pp. 95–118.
[30]S. K. Watson and R. O. Pohl, Phys. Rev. B **68**, 104203 (2003).
[31]C. Jin and J. Wetzel, Proceedings of the IEEE 2000 International Interconnect Technology Conference, 5–7 June 2000, pp. 99–101.
[32]R. M. Costescu, A. J. Bullen, G. Matamis, K. E. O'Hara, and D. G. Cahill, Phys. Rev. B **65**, 094205 (2002).
[33]A. Wolf and R. Brendel, Thin Solid Films **513**, 385 (2006).
[34]S. Gomes, L. David, V. Lysenko, A. Descamps, T. Nychyporuk, and M. Raynaud, J. Phys. D: Appl. Phys. **40**, 6677 (2007).
[35]D. W. Song, W.-N. Shen, B. Dunn, C. D. Moore, M. S. Goorsky, T. Radetic, R. Gronsky, and G. Chen, Appl. Phys. Lett. **84**, 1883 (2004).
[36]D. G. Cahill, Rev. Sci. Instrum. **61**, 802 (1990).
[37]D. J. Taylor, P. F. Fleig, and S. L. Hietala, Thin Solid Films **332**, 257 (1998).
[38]N. Hutchinson, T. Coquil, A. Navid, and L. Pilon, "Effective optical properties of highly ordered mesoporous thin tilms," Thin Solid Films (to be published).
[39]D. Fattakhova-Rohlfing, M. Wark, T. Brezesinski, B. M. Smarsly, and J. Rathousk, Adv. Funct. Mater. **17**, 123 (2007).
[40]S. B. Jung and H. H. Park, Thin Solid Films **494**, 320 (2006).
[41]B. Smarsly and M. Antonietti, Eur. J. Inorg. Chem. **2006**(6), 1111 (2006).
[42]D. Zhao, P. Yang, D. I. Margolese, B. F. Chmelkab, and G. D. Stucky, Chem. Commun. (Cambridge) **1998**, 2499.
[43]B. Smarsly, C. Goltner, M. Antonietti, W. Ruland, and E. Hoinkis, J. Phys. Chem. B **105**, 831 (2001).
[44]N. Kitazawa, H. Namba, M. Aono, and Y. Watanabe, J. Non-Cryst. Solids **332**, 199 (2003).
[45]S. Dourdain, A. Mehdi, J. F. Bardeau, and A. Gibaud, Thin Solid Films **495**, 205 (2006).
[46]P. Charbonneau and B. Knapp, PIKAIA, High Altitude Observatory, National Center for Atmospheric Research, Boulder, CO (http://www.hao.ucar.edu/Public/models/pikaia/pikaia.html), 2002.
[47]M. Braun and L. Pilon, Thin Solid Films **496**, 504 (2005).
[48]D. E. Aspnes, Am. J. Phys. **50**, 704 (1982).
[49]A. Majumdar, ASME J. Heat Transfer **115**, 7 (1993).
[50]O. Nilsson, O. Sandberg, and G. Bäckström, Rev. Sci. Instrum. **57**, 2303 (1986).
[51]D. G. Cahill, in *Microscale Energy Transport*, edited by C. L. Tien, A. Majumdar, and F. M. Gerner (Taylor & Francis, Washington, DC, 1997), pp. 95–118.
[52]M. Kaviany, *Principles of Heat Transfer in Porous Media* (Springer, New York, 1995).
[53]T. Yamane, N. Nagai, S. I. Katayama, and M. Todoki, J. Appl. Phys. **91**, 9772 (2002). 3ω
[54]S. M. Lee and D. G. Cahill, J. Appl. Phys. **81**, 2590 (1997).
[55]G. T. A. Kovacs, *Micromachined Transducers Sourcebook* (McGraw-Hill, Boston, MA, 1998).
[56]A. S. Grove, *Physics and Technology of Semiconductor Devices*, 1st ed. (Wiley, New York, 1967).
[57]S. Shenogin, A. Bodapati, P. Keblinski, and A. J. H. McGaughey, J. Appl. Phys. **105**, 034906 (2009).
[58]A. Jagannathan, R. Orbach, and O. Entin-Wohlman, Phys. Rev. B **39**, 13465 (1989).
[59]J. L. Feldman, M. D. Kluge, P. B. Allen, and F. Wooten, Phys. Rev. B **48**, 12589 (1993).
[60]D. A. G. Bruggeman, Ann. Phys. **24**, 636 (1935).
[61]R. Landauer, J. Appl. Phys. **23**, 779 (1952).
[62]S.-M. Lee, G. Matamis, D. G. Cahill, and W. P. Allen, Microscale Thermophys. Eng. **2**, 31 (1998).
[63]C. L. Tien and K. Vafai, in *Thermophysics and Thermal Control*, edited by R. Viskanta (American Institute of Aeronautics and Astronautics, New York, 1978), pp. 135–148.
[64]C. Kittel, *Introduction to Solid State Physics*, 7th ed. (Wiley, New York, 1996).